

How to Cite:

Chandramouleeswaran, M., & Puviarasan, N. (2022). Intelligent bite marking analysis and classification using deep convolutional neural network based Xception model. *International Journal of Health Sciences*, 6(S3), 12440–12456. <https://doi.org/10.53730/ijhs.v6nS3.9490>

Intelligent bite marking analysis and classification using deep convolutional neural network based Xception model

M. Chandramouleeswaran

Assistant Professor/Programmer, Department of Computer and Information Science, Annamalai University, Chidambaram, Tamilnadu, India

*Corresponding author email: m_moulee@yahoo.com

Dr. N. Puviarasan

Professor & Head, Department of Computer and Information Science, Annamalai University, Chidambaram, Tamilnadu, India

Email: npuvi2410@yahoo.in

Abstract---Bite mark analysis and classification play a vital role in forensics. The recent advances in computer vision and deep learning models paves a way for the design of automated bite mark detection and classification process. This article focuses on the design of intelligent bite marking analysis and classification using deep convolutional neural network based Xception model. The major goal of the proposed model is to determine the appropriate class labels for the bite marked images. The proposed model initially intends to pre-process the bite marked images in different ways such as hair removal, median filtering based noise removal, and adaptive histogram based contrast enhancement. Besides, Chan Vese Segmentation approach is applied for segmenting the bite marked images. The data augmentation process is performed for increasing the count of images. In addition, Xception model is employed for the extraction of features. Finally, two machine learning (ML) classifications such as support vector machine (SVM) and logistic regression (LR) models are employed for image classification. For demonstrating the enhanced performance of the presented models, a set of simulations were carried out on their own dataset and the results ensured the betterment of the proposed model over the other existing models.

Keywords---bite marking, image classification, forensics, machine learning, deep learning, image segmentation.

Introduction

Bite marks are a form of 'patterned injury', which means that the configuration is caused by a certain object [1]. They are also known as tool marks. Also, it is described as a bite mark made by the human teeth on individual basis or along with other mouthparts. It can be seen in the dead individuals or the living, where an individual might be the perpetrator or victim of the crime. It might be formed at the time of child abuse, assault, or adult related to sex related crimes [2]. Also, it can be found in inanimate objects or food substances at the crime scene. Identification of crime is complicated and requires pain-staking effort by several agencies [3]. Advancements in forensic sciences have made crime detection scientifically possible. In the past, dental identification predates finger printing, the usage of bite mark analysis is emerging to be recognized and procedure is in the development process. Similar to fingerprint, the bite mark made by the teeth could be a tool for Detection [4].

Bite mark might be seen on nearly any surface of the body; certain site is related to some forms of assault. The shoulders, neck, and breasts are frequently bitten in a sexually motivated attack, whereas in child abuse cases, the buttocks and bites of the arms are common [5]. Adolescent self-inflicted bites may be found on the medial aspect of the arm. The American Board of Forensic Odontology for use in any bite mark analysis has made some guidance [6]. This guideline is considered dynamic and is being adapted as substantial development evolves so that the quality of investigation gets improved. Different techniques of analyzing bite marks are presented namely impression making from bitten substance by photocopying, computer-enabled overlay generation technique, photography method hand tracing, and dental stone from dental study cast [7]. The earlier study suggests that computer-generated overlays provide reproducible and more precise examples [8]. The major parameter of the investigation is the measurement of intercanine distance (ICD), as the impression of the anterior teeth is likely to be measurable and generally the most evident [9]. In recent times, deep learning (DL) model is extensively employed in image processing and computer vision applications. A convolution neural networks (CNN) convolve an input image with a determined weight matrix for extracting certain image feature without the loss of spatial arrangement data [10]. Initially, we estimate distinct structures for determining the optimally implementing CNN for the binary classification task and aims at accomplishing literature reported performance level.

Sun et al. [11] adapted the Grad-CAM technology for analyzing the tooth-marked tongue. Then, presented an approach that localizes the central region in the image to predict the pathology without bounding box and precisely categorizes tooth-marked tongue. By using the visual interpretation of tooth-mark problems, the study explored the effects of receptive field size on the classification result. Chintala et al. [12] performed detection of human bite marks on victim and analyzed with computer-based superimposition technology through Adobe Photoshop software. Five bite marks cases have been investigated in the literature. Dama et al. [13] aimed at exploring the degree of distortion among a 'bite marks' and a 'touch marks' on the left upper arm at 3 distinct positions (arm flexed; arm relaxed in 2 distinct locations).

A couple of dental casts using biting edges coated in ink were utilized for creating a mark in thirty subjects (6 ♂, 24 ♀) aged twenty to fifty years old. The photograph was captured by using Nikon DX digital camera (D5000). The mesiodistal angle and width of rotation of the inter-canine distance, lower and upper right central incisor were analyzed and comparison to the accurate measurement using Adobe Photoshop CC 2017. This study develops an intelligent bite marking analysis and classification using deep convolutional neural network based Xception model. Primarily, the proposed model undergoes preprocessing in different ways such as hair removal, median filtering based noise removal, and adaptive histogram based contrast enhancement. Moreover, Chan Vese Segmentation approach is applied for segmenting the bite marked images. Additionally, Xception model is employed for the extraction of features. Furthermore, two machine learning (ML) classification as support vector machine (SVM) and logistic regression (LR) models are employed for image classification. For demonstrating the enhanced performance of the proposed models, a set of simulations are executed on own dataset.

The Proposed Model

In this article, a new bite marking classification model has been developed to determine the appropriate class labels for the bite marked images. The proposed model performs different stages of operations such as pre-processing, Chan Vese based image segmentation, Xception feature extraction, and classification. The detailed work of each module is offered in the succeeding sections. Fig. 1 illustrates the overall process of proposed method.

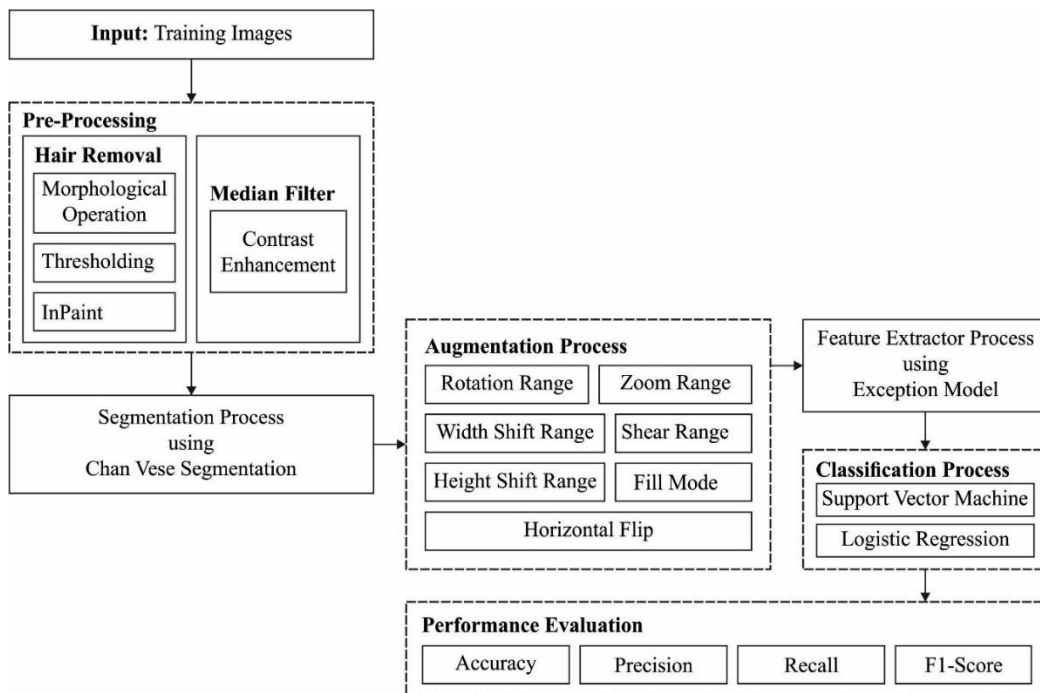


Fig. 1. Overall process of proposed method

Pre-processing

At the first stage of pre-processing, hair removal process is performed using black hat filtering. In morphology and digital image processing, top-hat and black-hat transforms are generally employed for extracting artefacts and details from the provided images. The black hat transform is represented by the difference between the closing image and input image. In this work, it is applied to remove the presence of minute hairs that exist in the bite marked skin regions. Followed by, median filtering (MF) approach is used for removing the noise that exists in the bite mark image. MF approach is a non-linear procedure helpful for decreasing impulsive, or salt-and-pepper noise. It can be also helpful from preserve edge from an image but decreasing arbitrary noise. Afterward, adaptive histogram equalization (AHE) is a digital image processing approach utilized for enhancing the contrast of images. It varies in normal HE from the respect that adaptive technique improves the contrast locally. It splits the image as to various blocks and calculates HE to all the sections. Therefore, AHE computes several histograms, all equivalent to various sections of images. It improves the local contrast and definition of edges from every different region of images.

Image Segmentation using Chan Vese Approach

While segmenting images to determine the bite marked regions, the Chan Vese approach is applied to pre-processed images. Consider $f(x) = (x_1, x_2) \in \Omega \subset \mathbb{R}_t^2$ denotes the input image that should be segmentation. The generalized image segmentation problem using the Mumford-Shah image technique:

$$\min \mu H^1(C) + \lambda \int_{\Omega} (f - u)^2 dx + \int_{\Omega \setminus C} |\nabla u|^2 dx, \quad (1)$$

Whereas C denotes an edge set, u indicates a differentiable function on $\Omega \setminus C$, H^1 shows the 1D Hausdorff measure, $\nabla u = (u_{x_1}, u_{x_2})$ signifies the gradient operator, $|\cdot|$ denotes the L^2 norm and parameter $\mu > 0, \lambda > 0$.

In Eq. (1), assume that C denotes the closed curve, the 1D Hausdorff measure of C gets curve length. It can be expressed as follows:

$$\operatorname{argmin}_{u,C} \mu \operatorname{length}(C) + \lambda \int_{\Omega} (f - u)^2 dx + \int_{\Omega \setminus C} |\nabla u|^2 dx. \quad (2)$$

Assume that the function:

$$u(x) = \begin{cases} c_{12} & \text{if } x \in C \\ c_{22} & \text{if } x \notin C \end{cases}$$

We acquire the subsequent model:

$$\operatorname{arg} \min_{c_1, c_2, C} \mu \operatorname{length}(C) + v \operatorname{Area}(C) + \lambda_1 \int_{x \in C} |f - c_1|^2 dx + \lambda_2 \int_{x \notin C} |f - c_2|^2 dx_t \quad (3)$$

In which, length (C) indicates the length of curve C , Area (C) represent the area inside C , parameter $\mu > 0, v > 0, \lambda_1 > 0, \lambda_2 > 0$. Eq. (3) is named as Chan-Vese image segmentation method. The aim of presented approach is to discover the optimal u fitting f by minimalizing the abovementioned energy function. In Eq. (3), the 1st term represents the regularity by the curve length, the 2nd term-penalize the enclosed area of C for controlling its size, the 3rd and 4th term penalize discrepancy among the input image f and the piecewise constant function u .

Data augmentation

To increase the number of images in the training and testing dataset, data augmentation process is employed. In this work, data augmentation takes place in different ways such as listed below.

- rotation_range = 20
- zoom_range = 0.15
- width_shift_range = 0.2
- height_shift_range = 0.2
- shear_range = 0.15
- horizontal_flip = True
- fill_mode = "nearest"

Feature Extraction using Xception Model

During feature extraction process, the segmented images are passed into the Xception model to produce feature vectors. The constant development of deep learning (DL) of CNN has enhanced the architecture for precise image classifier approaches. Likewise, Xception model was proposed under some major concepts including depthwise separable Conv layer, Conv layer, residual connection, and inception module. As well, CNN model for the activation function is needed. Xception [14] is determined as a hypothesis-based Inception architecture that creates correlation of cross-channel and spatial relation within feature map of CNN able to be decoupled fully. Extreme or Xception version of the inception architecture is a pre-trained neural network that functions on depth-wise separable Conv. In depth-wise Conv, channel-wise $n \times n$ spatial Conv has been implemented, whereas, in the revised version (Xception), point-wise Conv is followed by depth-wise Conv [15]. It is depending on the statement that the correlations among the input channels are fully separable from the spatial correlations. Especially, Xception extended the inception model by replacing typical Conv with depth-wise independent Conv. Fig. 2 shows the architecture of Xception Model.

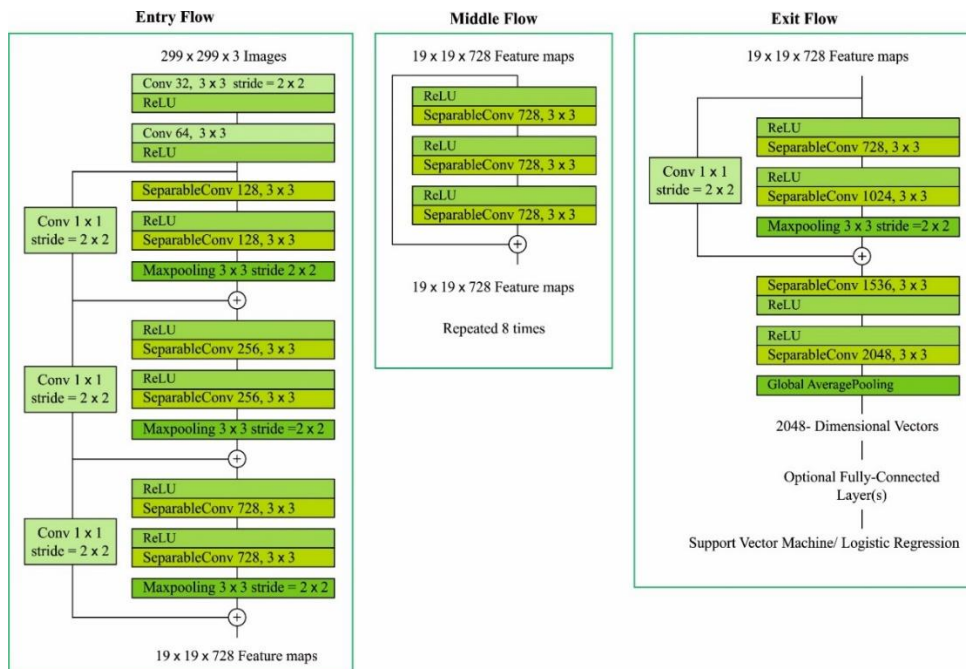


Fig. 2. Architecture of Xception Model

In employing Conv layers inside the Xception model, there is layer after the input layer, which generates Conv kernel to estimate distinct feature maps to illustrate the feature of the input data. To generate feature map, the Conv kernel is separated into each area of the input data. The important layer of Xception is the depthwise separable Conv. This could minimize the model parameters and computation that is ordered in the spatial dimension and depth dimension of color channel. This can be done by separating from the conventional Conv operation more deeply with depthwise Conv connected to point-wise Conv by generating a Conv kernel size of 1×1 , that operate depthwise separable Conv.

Image Classification

At the final stage, the extracted features are passed into two ML models for classification purposes. LR technique is the generalized linear model (GLM). It is utilized for binary variables whereby the response records failure or success for a presented event. It can be expressed in the following equation [16]

$$p_j = f(y|x) = \frac{1}{1 + \exp \{-(\beta_0 + \beta_1 x_i)\}} \quad (4)$$

Whereas p_j denotes the possibility of success and, $P(y_j = 1) = p_j$ and $P(y_j = 0) = q_j = 1 - p_j$, $0 \leq p_j \leq 1$. As well, β_0 and β_1 indicates the parameter, x_j shows an independent variable, \exp represent the arithmetical constant named Euler number that nearly equivalent to 2.78. The LR could be expanded to integrate one or two independent variables, that is categorical or continuous variables. The multiple LR is formulated by:

$$p_i = \frac{1}{1 + \exp\{-z_i\}} = \frac{\exp\{z_i\}}{1 + \exp\{z_i\}} \quad (5)$$

Whereas, $z_i = \beta_0 + \beta_1 x_1 + \beta_2 x_2 + \dots + \beta_n x_n$ and $\frac{p_i}{1-p_i} = \frac{1 + \exp\{z_i\}}{1 + \exp\{-z_i\}} = \exp\{z_i\}$. in which, $\frac{p_i}{1-p_i}$ indicates the odd ratio determined as the possibility of existence of the event separated by the probability of not existence the event [17].

$$p_i = \frac{\text{odds}}{1 + \text{odds}} = \frac{\exp\{\beta_0 + \beta_1 x_1 + \beta_2 x_2 + \dots + \beta_n x_n\}}{1 + \exp\{\beta_0 + \beta_1 x_1 + \beta_2 x_2 + \dots + \beta_n x_n\}} \quad (6)$$

$$\text{logit} = \ln(\text{odds}) = \ln\left(\frac{p_i}{1-p_i}\right) = z_j \quad (7)$$

$$\text{logit} = \beta_0 + \beta_1 x_1 + \beta_2 x_2 + \dots + \beta_n x_n, \quad -\infty < \text{logit} < \infty \quad (5)$$

Thus, logit is a linear function in independent variable $x_j, 1 \leq j \leq n$.

SVM model is dependent upon the model of fundamental risk minimized and statistical learning model. According to the trained data, the aim of SVM classification is to forecast of class label to that an instance fits. In recent times, SVMs are widely executed for medical analysis problems to identify any potential risk factors or cause connected to disease [18]. Usually, this technique was utilized to 2 class discrimination problems connected to instances going to +1 (positive) and -1(negative) class labels. In order to classify the data, SVM generates a hyperplane from n -dimension feature space for providing an optimum separation. While there are several valid hyperplanes, the phenomenal properties of SVM are that it attempts for identifying a better separate hyperplane $f(x): w^T x + b = 0$ from the feature spaces with maximized the margin amongst the 2 classes, for instance, diseased *vs.* normal. The instances that lie neighboring to optimum hyperplane are mentioned that the support vector.

The trained instance is provided by $(x_i, y_i), i \in I = \{1, 2, \dots, S\}$, whereas $y_i = \{+1, -1\}$ signifies the class of instance $x_i \in \mathcal{R}^n$, n stands for the amount of features from all samples and S refers the amount of trained instances. An optimum separate hyperplane is provided in Eq. (8)

$$y = \text{sign}[w^T \phi(x_i) + b] \quad (8)$$

which is attained by resolving the subsequent quadratic programming problem (QPP) provided in Eq. (9)

$$\min_{w, b, \xi} \frac{1}{2} w^2 + C \sum_{i=1}^S \xi_i \quad (9)$$

subject to $y_i(w^T \phi(x_i) + b) \geq 1 - \xi_i$, Where $\xi_i \geq 0, \forall i = 1, 2, \dots, S$.

At this point, b signifies the bias, $w \in \mathcal{F}$ stands for the weight vector of optimum hyperplane within the altered feature space \mathcal{F} , ξ_i implies the surplus variable representing the error connected to i^{th} instance margin interms of the separate hyperplane [19], C implies the regularization parameter that controls the

misclassification cost of samples and penalizes ξ_i , $C > 0$. With the overview of non-negative Lagrange multiplier α_i , Eq. (9) is resolved in dual-form as signified as the subsequent QPP in Eq. (10)

$$\max_{\alpha_i} \sum_{i=1}^s \alpha_i - \frac{1}{2} \sum_{i,j=1}^s \alpha_i \alpha_j y_i y_j K(x_i, x_j) \quad (10)$$

subject to $\sum_{i=1}^s \alpha_i y_i = 0$, where $0 \leq \alpha_i \leq C$, $\forall i = 1, 2, \dots, S$.

With $C > 0$, $\alpha_i = [\alpha_1, \alpha_2, \dots, \alpha_S]^T$ defines the coefficients equivalent to x_i with support vector (SV) demonstrating every x_i with non-zero α_i . The resultant optimum decision function has represented as Eq. (11)

$$y_i = \text{sign} \left(\sum_{i=1}^s \alpha_i y_i K(x_i, x_j) + b \right) \quad (11)$$

where $x = [x_1, x_2, \dots, x_S]$ implies the input data, α_i and y_i represents the Lagrange multiplier. An unseen testing sample x is forecasted utilizing in Eq. (11). At this point, $K(x_i, x_j)$ refers the Gaussian radial basis kernel function, formulated as $(x_i, x_j) = \exp \left(-x_i - \frac{x_j^2}{2\gamma^2} \right)$, $\gamma > 0$. This kernel function generate an SVM applicable to nonlinear cases. During this case, to resolve the binary classifier problems the RBF kernel was employed that is always the primary choice for an SVM application.

Results and Discussion

For experimental validation, we have collected a set of bite marked images on our own. The dataset holds images under 12 class labels with 2 images under every class. Fig. 3 visualizes the sample results obtained by the proposed model at the preprocessing and segmentation stages. Fig. 3a illustrates the original input images and the respective preprocessed and segmented versions are shown in Figs. 3b and 3c respectively.

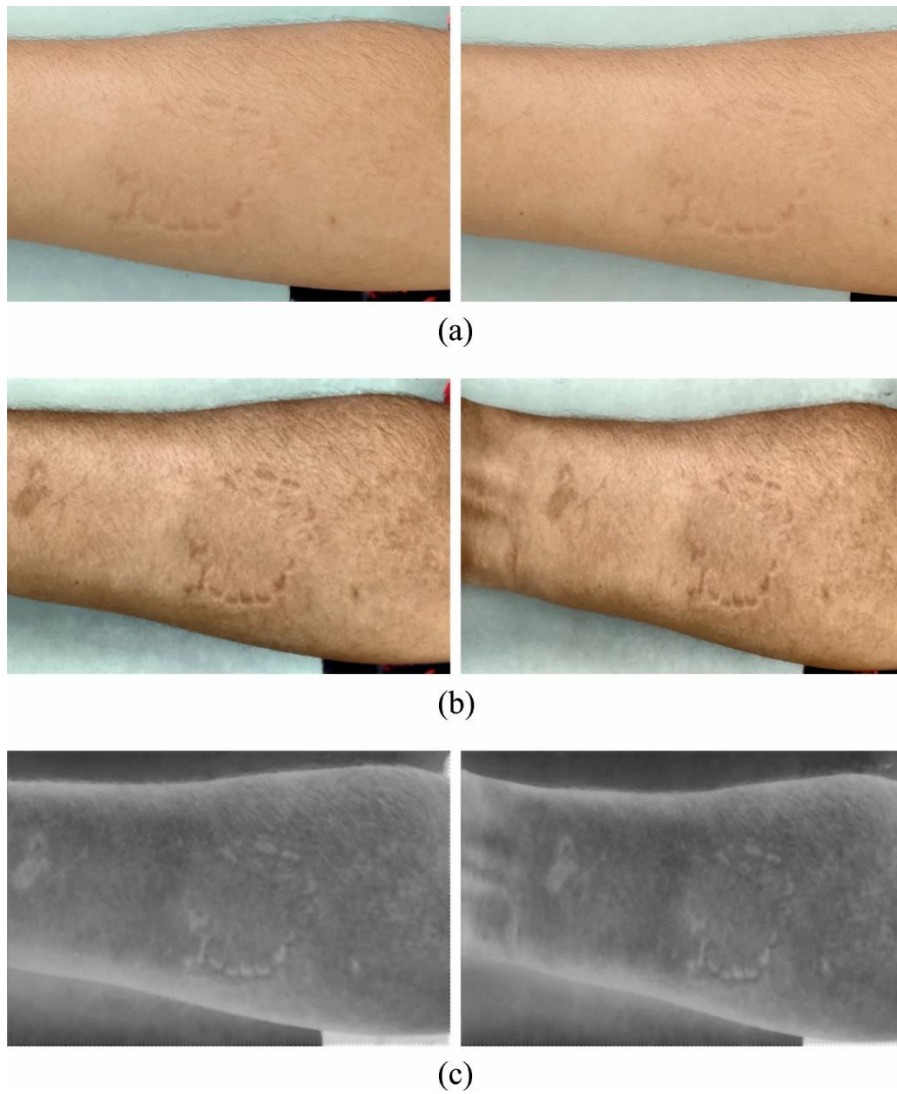


Fig. 3. a) Original Images b) Preprocessed Images c) Segmented Images

During the data augmentation process, two images in each class are increased to 32 images under each class. Therefore, the augmented dataset holds 384 images with 32 images under every class.

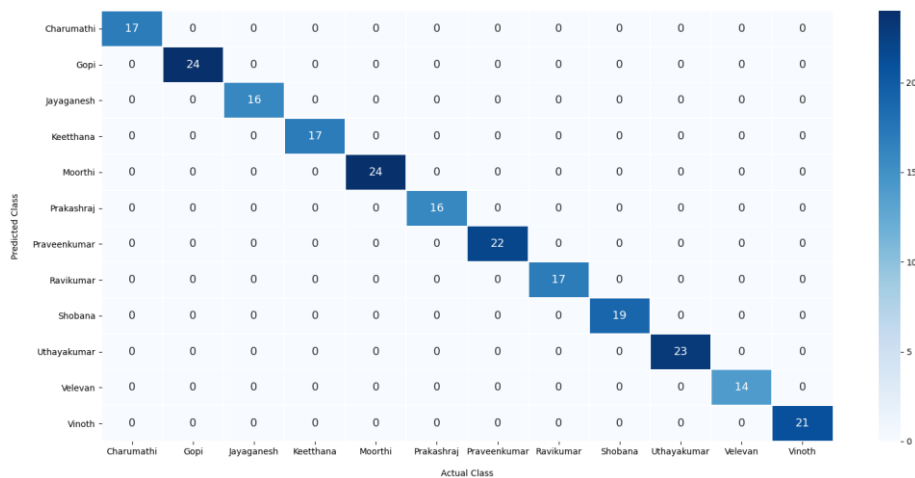


Fig. 4. Confusion matrix of Xception-SVM (Training Phase)

Fig. 4 portrays the confusion matrix generated by the Xception-SVM model in the training phase. The figure reported that the Xception-SVM model has identified 17 images into class 1, 24 images into class 2, 16 images into class 3, 17 images into class 4, 24 images into class 5, 16 images into class 6, 22 images into class 7, 17 images into class 8, 19 images into class 9, 23 images into class 10, 14 images into class 11, and 21 images into class 12.

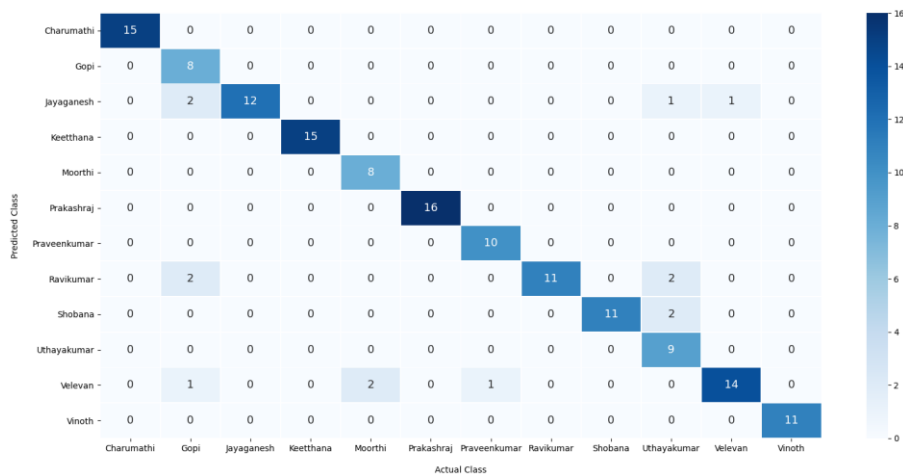


Fig. 5. Confusion matrix of Xception-SVM (Testing Phase)

Fig. 5 represents the confusion matrix generated by the Xception-SVM model on the testing stage. The figure described that the Xception-SVM model has recognized 15 images into class 1, 8 images into class 2, 12 images into class 3, 15 images into class 4, 8 images into class 5, 16 images into class 6, 10 images into class 7, 11 images into class 8, 11 images into class 9, 9 images into class 10, 14 images into class 11, and 11 images into class 12.

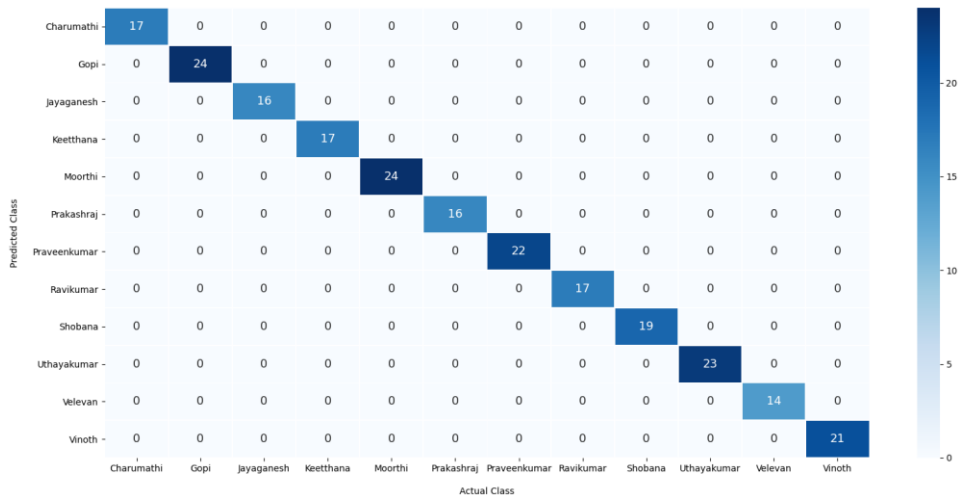


Fig. 6. Confusion matrix of Xception-LOR (Training Phase)

Fig. 6 depicts the confusion matrix generated by the Xception-LOR model on the training stage. The figure described that the Xception-LOR model has identified 17 images into class 1, 24 images into class 2, 16 images into class 3, 17 images into class 4, 24 images into class 5, 16 images into class 6, 22 images into class 7, 17 images into class 8, 19 images into class 9, 23 images into class 10, 14 images into class 11, and 21 images into class 12.

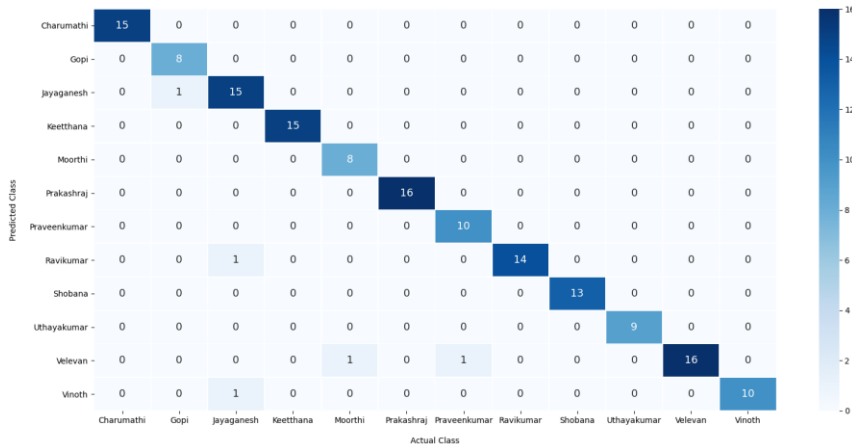


Fig. 7. Confusion matrix of Xception-LOR (Testing Phase)

Fig. 7 represents the confusion matrix generated by the Xception-LOR model on the testing stage. The figure described that the Xception-LOR model has identified 15 images into class 1, 8 images into class 2, 15 images into class 3, 15 images into class 4, 8 images into class 5, 16 images into class 6, 10 images into class 7, 14 images into class 8, 13 images into class 9, 9 images into class 10, 16 images into class 11, and 10 images into class 12. Table 1 and Fig. 8 reports the overall bite marking classification outcomes of the Xception-SVM and Xception-LOR models. The results show that the Xception-SVM model has accomplished $accu_y$, $prec_n$, $reca_l$, and $F1_{score}$ of 90.91%, 90.84%, 92.56%, and 90.45%

respectively. On the other hand, the Xception-LOR model has resulted to $accu_y$, $prec_n$, $reca_l$, and $F1_{score}$ of 96.75%, 96.41%, 97.24%, and 96.69% respectively.

Table 1
Result analysis of proposed model with different measures

Methods	Accuracy (%)	Precision (%)	Recall (%)	F1-Score (%)
Xception-SVM	90.91	90.84	92.56	90.45
Xception-LOR	96.75	96.41	97.24	96.69

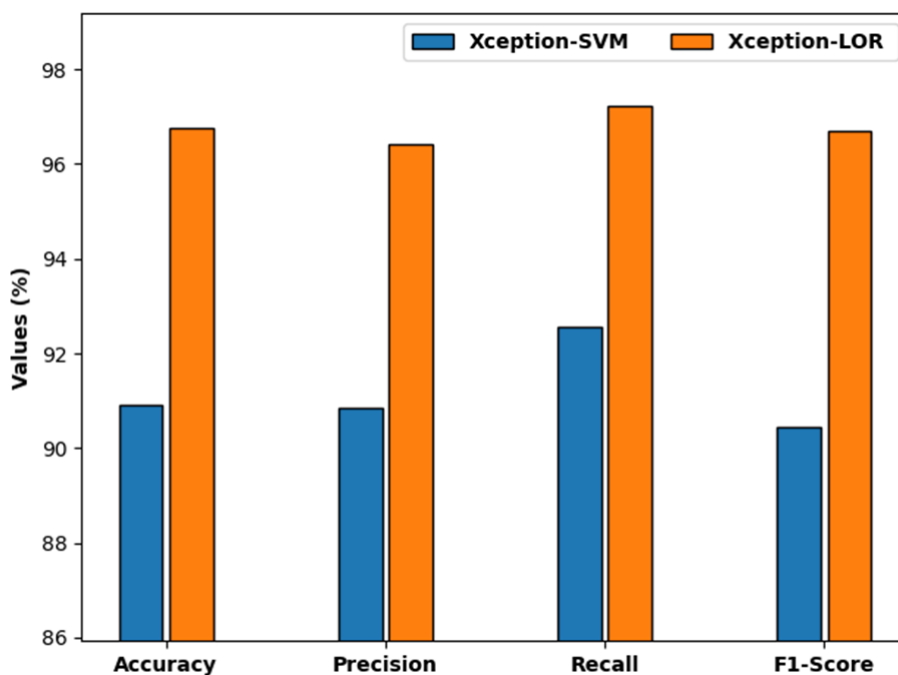


Fig. 8. Result analysis of proposed model with different measures

Table 2 portrays an overall comparative study of the proposed models with existing models. The results indicated that the presented Xception-SVM and Xception-LOR models have shown effectual outcomes over the other methods.

Table 2
Comparative analysis of proposed method with recent approaches

Methods	Precision	Recall	Accuracy	F-Score
CNN Layer-3	0.7040	0.6210	0.7130	0.6600
CNN Layer-4	0.7700	0.5610	0.7360	0.6500
CNN Layer-5	0.7590	0.7810	0.7860	0.7700
CNN Layer-6	0.7250	0.6770	0.7210	0.7000
Xception-SVM	0.9084	0.9256	0.9091	0.9045
Xception-LOR	0.9641	0.9724	0.9675	0.9669

Fig. 9 provides a brief $prec_n$ inspection of the Xception-SVM and Xception-LOR models with existing techniques. The results indicated that the CNN Layer-3 model has shown poor results with the least $prec_n$ of 0.7040. Followed by, the CNN Layer-6 model has resulted in slightly enhanced $prec_n$ of 0.7250. At the same time, the CNN Layer-5 model has reached moderately increased $prec_n$ of 0.7590%. Though the CNN Layer-4 model has accomplished reasonably $prec_n$ of 0.7700, the presented Xception-SVM and Xception-LOR models have reached superior performance with the $prec_n$ of 0.9084 and 0.9641.

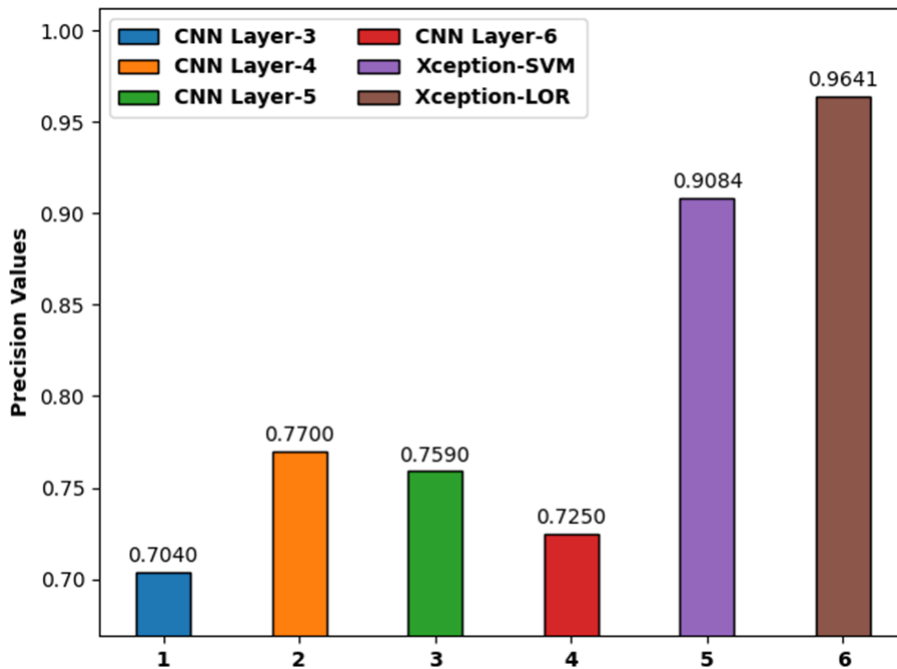


Fig. 9. $prec_n$ analysis of proposed method with recent approaches

Fig. 10 offers a brief $reca_l$ inspection of the Xception-SVM and Xception-LOR models with current methods. The results designated that the CNN Layer-3 model has shown poor outcomes with the least $reca_l$ of 0.6210. After that, the CNN Layer-6 model has resulted in slightly enhanced $reca_l$ of 0.6770. Simultaneously, the CNN Layer-5 model has reached moderately increased $reca_l$ of 0.7810%. Though the CNN Layer-4 model has attained reasonable $reca_l$ of 0.5610, the presented Xception-SVM and Xception-LOR models have reached higher performance with the $reca_l$ of 0.9256 and 0.9724.

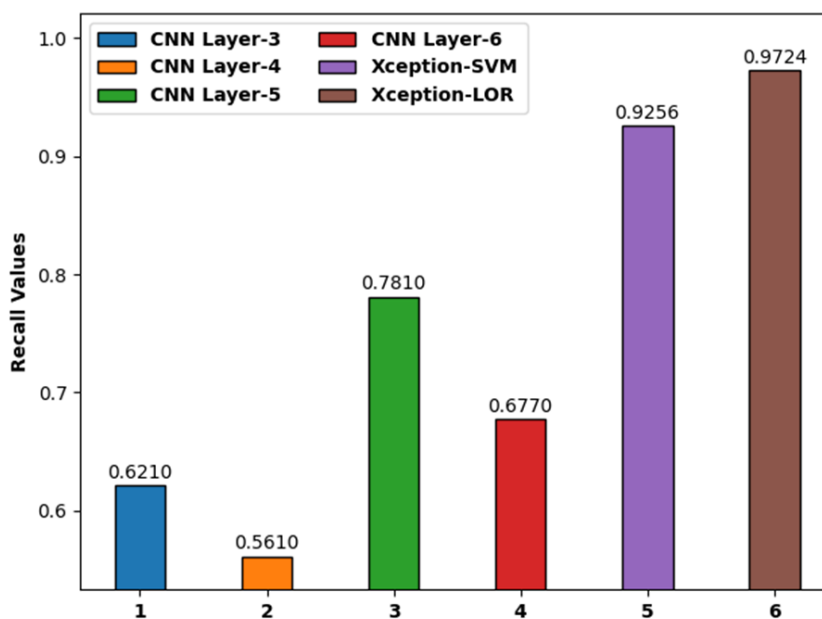


Fig. 10. $Recall_i$ analysis of proposed method with recent approaches

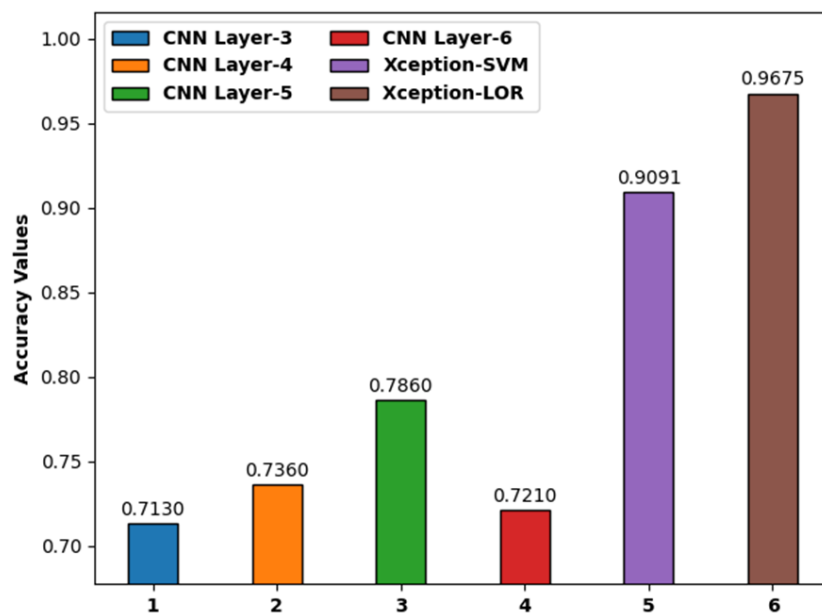


Fig. 11. Acc_y analysis of proposed method with recent approaches

Fig. 11 shows a brief acc_y inspection of the Xception-SVM and Xception-LOR models with present methods. The results show that the CNN Layer-3 model has revealed poor outcomes with the least acc_y of 0.7130. Followed by, the CNN Layer-6 model has resulted in slightly enhanced acc_y of 0.7210. Simultaneously, the

CNN Layer-5 model has reached moderately increased acc_y of 0.7560%. Though the CNN Layer-4 model has gained reasonable acc_y of 0.7360, the presented Xception-SVM and Xception-LOR models have reached greater performance with the acc_y of 0.9091 and 0.9675.

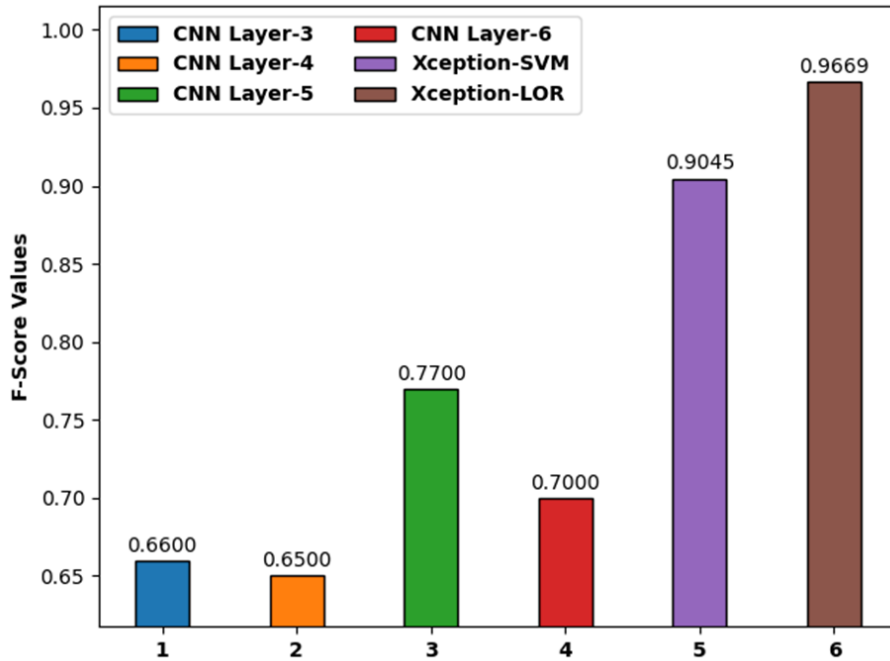


Fig. 12. F_{score} analysis of proposed method with recent approaches

Fig. 12 illustrates a brief F_{score} inspection of the Xception-SVM and Xception-LOR models with current approaches. The results showed that the CNN Layer-3 model has revealed poor results with the least F_{score} of 0.6600. After that, the CNN Layer-6 model has resulted in slightly enhanced F_{score} of 0.7000. Simultaneously, the CNN Layer-5 model has gained moderately increased F_{score} of 0.7700%. Though the CNN Layer-4 model has gained reasonable F_{score} of 0.6500, the existing Xception-SVM and Xception-LOR models have reached larger performance with the F_{score} of 0.9045 and 0.9669. From the detailed results and discussion, it is ensured that the Xception-SVM and Xception-LOR models have outperformed the existing methods on bite marking classification. Particularly, the Xception-LOR model has resulted to superior results with the maximum acc_y of 0.9675. Therefore, it can be utilized as a proficient tool for bite marking classification.

Conclusion

In this article, a new bite marking classification model has been developed to determine the appropriate class labels for the bite marked images. The proposed model performs different stages of operations such as pre-processing, Chan Vese based image segmentation, Xception feature extraction, and classification. In addition, Chan Vese Segmentation approach is applied for segmenting the bite

marked images. At last, Xception model with two ML models such as SVM and LR models are employed for image classification. For demonstrating the enhanced performance of the proposed models, a set of simulations were carried out on their own dataset and the results ensured the betterment of the proposed model over the other existing models. In future, deep instance segmentation models can be designed to improve the bite mark classification performance.

References

1. Maji, A., Khaitan, T., Sinha, R., Sarkar, S., Verma, P. and Shukla, A.K., 2018. A novel computer-assisted method of bite mark analysis for gender determination. *Journal of environmental and public health*, 2018.
2. K. Bhargava, D. Bhargava, P. Rastogi et al., "An overview of bite mark analysis," *Journal of Indian Academy of Forensic Medicine*, vol. 34, no. 1, pp. 61–66, 2012.
3. M. J. Daniel, N. Bhardwaj, S. V. Srinivasan, V. K. Jimsha, and F. Marak, "Comparative study of three different methods of overlay generation in bite mark analysis," *Journal of Indian Academy of Forensic Medicine*, vol. 37, no. 1, pp. 24–28, 2015.
4. L. Chintala, M. Manjula, S. Goyal, V. A. Chaitanya, M. K. Hussain, and Y. C. Chaitanya, "Human bite marks—a computer-based analysis using adobe photoshop," *Journal of Indian Academy of Oral Medicine and Radiology*, vol. 30, no. 1, pp. 58–63, 2018.
5. Li, W.; Luo, J.; Hu, S.; Xu, J.; Zhang, Z. Towards the Objectification of Tongue Diagnosis: the Degree of Tooth-marked. In *Proceedings of the IEEE International Symposium on It in Medicine and Education*, Xiamen, China, 12–14 December 2008; pp. 592–595.
6. Ren, Y.; Rong, L.; Ying, Z. Study on the correlation between dental scar tongue and constitution of traditional Chinese medicine in physical examination population. *World Sci. Technol.-Mod. Tradit. Chin. Med.* 2012, 14, 2283–2289.
7. Li, X.; Yin, Z.; Cui, Q.; Yi, X.; Yi, Z. Tooth-Marked Tongue Recognition Using Multiple Instance Learning and CNN Features. *IEEE Trans. Cybern.* 2019, 49, 380–387.
8. Wang, Y.G.; Yang, J.; Zhou, Y.; Wang, Y.Z. Region partition and feature matching based color recognition of tongue image. *Pattern Recognit. Lett.* 2007, 28, 11–19.
9. Pang, B.; Zhang, D.; Li, N.; Wang, K. Computerized tongue diagnosis based on Bayesian networks. *IEEE Trans. Biomed. Eng.* 2004, 51, 1803–1810.
10. K. S. Gopal and A. V. Anusha, "Evaluation of accuracy of human bite marks on skin and an inanimate object: a forensicbased cross-sectional study," *International Journal of Forensic Odontology*, vol. 3, no. 1, pp. 2–5, 2018.
11. Sun, Y., Dai, S., Li, J., Zhang, Y. and Li, X., 2019. Tooth-marked tongue recognition using gradient-weighted class activation maps. *Future Internet*, 11(2), p.45.
12. Chintala, L., Manjula, M., Goyal, S., Chaitanya, V., Hussain, M.K.A. and Chaitanya, Y.C., 2018. Human bite marks—a computer-based analysis using adobe photoshop. *Journal of Indian Academy of Oral Medicine and Radiology*, 30(1), p.58.

13. Dama, N., Forgie, A., Mânica, S. and Revie, G., 2020. Exploring the degrees of distortion in simulated human bite marks. *International journal of legal medicine*, 134(3), pp.1043-1049.
14. Chollet, F. Xception: Deep learning with depthwise separable Convs. arXiv 2016, arXiv:1610.02357.
15. Jinsakul, N., Tsai, C.F., Tsai, C.E. and Wu, P., 2019. Enhancement of deep learning in image classification performance using xception with the swish activation function for colorectal polyp preliminary screening. *Mathematics*, 7(12), p.1170.
16. Hosmer Jr, D. W., Lemeshow, S., & Sturdivant, R. X. (2013). *Applied logistic regression* (Vol. 398). John Wiley & Sons.
17. Jawa, T.M., 2022. Logistic regression analysis for studying the impact of home quarantine on psychological health during COVID-19 in Saudi Arabia. *Alexandria Engineering Journal*.
18. B. Scholkopf, A.J. Smola, *Learning with Kernels: Support Vector Machines, ϵ Regularization, Optimization, and beyond*, MIT Press, 2002.
19. Singh, N. and Singh, P., 2021. A hybrid ensemble-filter wrapper feature selection approach for medical data classification. *Chemometrics and Intelligent Laboratory Systems*, 217, p.104396.
20. Suryasa, I. W., Rodríguez-Gámez, M., & Koldoris, T. (2021). Health and treatment of diabetes mellitus. *International Journal of Health Sciences*, 5(1), i-v. <https://doi.org/10.53730/ijhs.v5n1.2864>
21. Suryasa, I. W., Rodríguez-Gámez, M., & Koldoris, T. (2021). The COVID-19 pandemic. *International Journal of Health Sciences*, 5(2), vi-ix. <https://doi.org/10.53730/ijhs.v5n2.2937>
22. Mustafa, A. R., Ramadany, S., Sanusi, Y., Made, S., Stang, S., & Syarif, S. (2020). Learning media applications for toddler midwifery care about android-based fine motor development in improving midwifery students skills. *International Journal of Health & Medical Sciences*, 3(1), 130-135. <https://doi.org/10.31295/ijhms.v3n1.290>